8 Introduction to Topological Phases in Condensed Matter

Cécile Repellin
LPMMC, CNRS, Université Grenoble Alpes
25 avenue des Martyrs, 38000 Grenoble, France

Contents

E. Pavarini and E. Koch (eds.)
Correlated Materials: Methods and Applications
Modeling and Simulation Vol. 16, Forschungszentrum Jülich, 2026
ISBN 978-3-95806-909-1 http://www.cond-mat.de/events/correl26

Topological phases of matter are an extremely rich and active field of research. The first topological phase of matter ever observed was the integer quantum Hall effect, which was first observed by von Klitzing in 1980 [1]. Yet, it is only with the theoretical understanding of topology as an organizing principle of phases of matter in the 2000s that the field really started to blossom. Along with theoretical progress came the discovery of new materials, and the realization that many known materials are in fact topological. Topological phases are comprised of phases as varied as insulators, semimetals, and superconductors, and are observed in any dimension. They reach many experimental fields, from bulk 3D materials to two-dimensional heterostructures, thin films, as well as synthetic quantum matter, such as cold atoms in optical lattices, photonic systems, Josephson junction arrays ... As they apply to all wave phenomena, the same topological unifying principles also describe non-quantum systems, from oceanic waves to active matter, or mechanical resonators. These lectures notes focus on non-interacting topological insulators in two-dimensional quantum systems, and more specifically on the example of the Chern insulator. In Sec. 1, we give a very qualitative introduction to topological phases of matter by presenting it as an organizing principle in condensed matter. In Sec. 2–3, we define core mathematical concepts of topology, such as the Berry phase, Berry curvature and Chern number, and highlight their relevance to some physical quantities. Finally, in Sec. 4, we detail a few paradigmatic models of Chern insulators, introducing some of the microscopic ingredients allowing topology to emerge, and highlight their relevance to solid state and cold atom experiments.

1 Organizing principles in condensed matter

Understanding the world through the lens of physics often means looking for universality: unifying principles, which describe many phenomena regardless of the physical system, its geometry, constituents, or scale. The emergence of universality is particularly striking in condensed matter, where phases of matter arise from the complex interactions between macroscopically many constituents, and similar phenomena can be observed in extremely varied materials.

1.1 Symmetry breaking

The concept of symmetry breaking is an immensely helpful organizing principle of phases of matter, describing crystals, magnets, superfluids, and more. It can be summarized like so: the low-temperature phase of a system is less symmetric than the Hamiltonian describing it. For example, the position of atoms in a crystalline solid breaks the continuous translation and rotation symmetry, which is restored at higher temperature, in the liquid and gas phases. Likewise, magnets form when the magnetization of a solid selects a preferential orientation, thus breaking rotational symmetry.

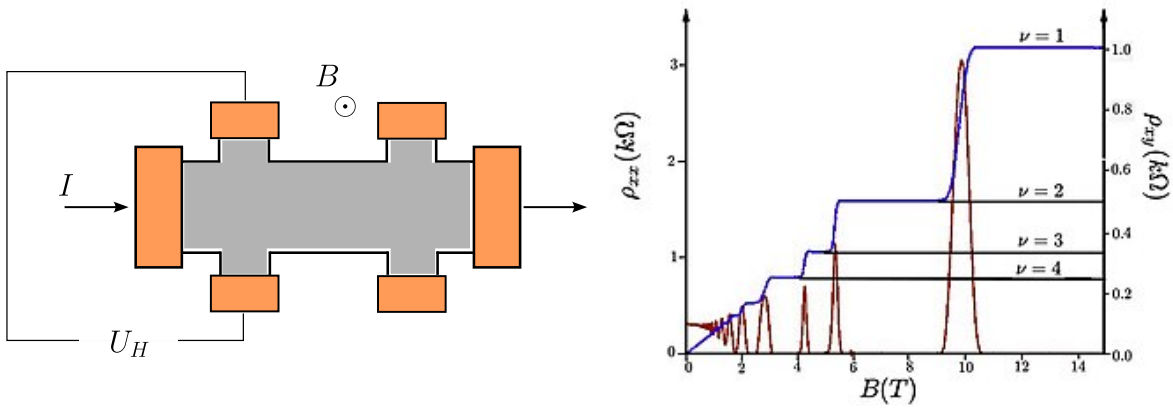

Fig. 1: *Integer quantum Hall effect. (Left) Set-up of a Hall experiment. A sample is placed in a magnetic field B, and a current I is imposed. A transverse or Hall voltage U_H is measured. (Right) Longitudinal and transverse (Hall) resistivity ρ_{xx} and $\rho_{xy} = U_H/I$, of a two-dimensional electron gas as a function of magnetic field. Both quantities were divided by the quantum unit of conductance e^2/h. Whenever $\rho_{xx} = 0$, the longitudinal conductance σ_{xx} vanishes as well, and the transverse resistance $\rho_{xy} = 1/\sigma_{xy}$ is quantized and forms a plateau. The integer ν is the ratio between electronic density and magnetic field (in units of the quantum of magnetic flux), and is known as the filling factor. It is equal to the Hall conductance in units of e^2/h. Figure reproduced from Wikipedia, The Quantum Hall Effect.*

1.2 The quantum Hall effect

While the concept of symmetry breaking describes a very large number of phases of matter, it fails (at least in its traditional formulation) to explain several phenomena. The integer quantum Hall effect, discovered in 1980 by Klaus von Klitzing [1] is the most emblematic, and historically the first such phenomenon. It describes the quantization of the transverse (or Hall) conductance σ_{xy} of a two-dimensional electron gas (2DEG) subjected to a perpendicular magnetic field (see Fig. 1)

$$\sigma_{xy} = n\,\frac{e^2}{h} = n\,\frac{1}{25812.807\,\Omega} \tag{1}$$

where n is an integer, and e and h are universal constants, respectively, the charge of the electron, and the Planck constant. Originally observed in silicon-based transistors at low temperature, it is often studied in gallium arsenide heterostructures, and is also observed in graphene at room temperature [2]. In spite of the important differences between these materials, and the inherent presence of disorder, which differs from sample to sample, the quantization occurring in the quantum Hall effect is expressed purely in terms of universal constants, and does not require any factor accounting for sample variety. It is also remarkably precise (up to the 9^{th} digit), which has made the integer quantum Hall effect the standard of metrology for measuring the quantum unit of conductance e^2/h.

1.3 Topological invariants and topological equivalence

The remarkable quantization of the integer quantum Hall effect is of course not by chance, but rather the result of the mathematical nature of the Hall conductance: when the longitudinal conductance vanishes (which occurs in the QHE), it is equal, in units of e^2/h, to a topological invariant which can only take integer values, the Chern number. This peculiar situation, where the longitudinal conductance vanishes, but the transverse one does not, is associated with a state which is insulating in the bulk of the system, with one-dimensional conducting channels at the edge. The edge channels are chiral (the direction of the magnetic field, or sign of the Chern number determines the direction of chirality), which protects them from any backscattering-induced gap opening. Loosely speaking, a topological invariant is a mathematical property of a space, which remains invariant under continuous transformations (homemorphisms). In the case of the Chern number as applied to condensed matter problems, continuous transformations are those which do not close the bulk gap of the system, i.e., the band gap, as Chern numbers describe materials well described by band theory. This gives an additional hint to explain the universality of the quantization of the Hall conductance across many materials and samples: there is a vast parameter space in which a band gap may remain open.
The robustness of topological phases is associated with the concept of topological equivalence. Two phases of matter are considered to be topologically equivalent if their topological invariant is equal, for example two insulators with equal Chern number. In other words, there is a smooth transformation connecting the two corresponding ground states. For insulators, this means, as already explained in the case of Chern insulators, that there exists a transformation connecting the two states, which does not close the gap. The notion of equivalence generalizes to metals: there exists a finite-depth quantum circuit connecting the two states, i.e., a product of local operators whose number remains finite in the thermodynamic limit. When a symmetry protects the topology (for example time-reversal symmetry in the case of $\mathbb{Z}_2$ topological insulators), one considers only local operators preserving the given symmetry to define topological equivalence.

1.4 Different types of topology

The realization that some topological invariants are connected to physical properties was a milestone in classifying phases of matter, and goes much beyond the connection between the Chern number and the Hall conductance. The Chern number is a property of insulators in 2 dimensions not preserving time-reversal symmetry. Two-dimensional insulators preserving time-reversal symmetry are characterized by a topological invariant taking only two possible values (0 or 1), a $\mathbb{Z}_2$ invariant, as was clarified by C. Kane and E. Mele [3]. The classification of topological phases extends to any dimension, and any symmetry in a table called the tenfold way [4], which holds for weakly interacting quantum matter. This is the context where band theory applies, and the topological invariant then characterizes the individual bands of a system. This type of topological phase of matter – *topological bands* – is to be clearly distinguished from the vastly different concept of *topological order*. A state with topological order is a gapped many-body state with a complex entanglement structure, which cannot be adiabati-

cally connected to a product of single-particle states (unlike, e.g., a Chern insulator). In turn, the elementary excitations are fractionalized: they are called anyons, and may carry a fractional charge and a fractional statistics (beyond bosons and fermions). Non-abelian anyons have an especially complex exchange statistics, which makes them promising for quantum computing technologies: they carry an intrinsic degeneracy, permitting logical gate operations, and the realization of qubits topologically immune to decoherence, in principle. The fractional quantum Hall effect is an example of a phase of matter with topological order (abelian or non-abelian depending on the fraction). In the context of frustrated magnetism, gapped spin liquids also carry topological order.

For a review of topological phases of matter, including the above examples, as well as semimetals, and topological defects in symmetry-breaking phases, we recommend the book by R. Moessner and J.E. Moore [5]. For a review of topological insulators and superconductors, see also the book by B.A. Bernevig and T. Hughes [6]. For a review of topological order and its link to quantum computation, see the review by Nayak *et al.* [7].

In the rest of these lecture notes, we will focus on one topological phase of matter, the Chern insulator (a two-dimensional insulator characterized by a Chern number). We will define the concepts of Berry phase, Berry connection, and Berry curvature necessary for its definition, and explain why it must be an integer. We will also go over some paradigmatic Chern insulator models, and highlight one very consequential conclusion from the connection between quantized Hall effect and Chern number: the possibility to have a quantized Hall conductance in the absence of a magnetic field.

2 Berry phase in quantum mechanics

The topological invariants characterizing topological phases of matter are geometric properties of the underlying quantum state. Here, we will start by defining the simplest geometric property of a quantum state, the Berry phase [8], which is the phase acquired by a quantum state after undergoing adiabatic evolution, independently of the energy of the quantum state, and is a simple consequence of the adiabatic theorem of quantum mechanics.

2.1 Definition of the Berry phase

Let us consider a quantum system described by a Hamiltonian H_λ, where λ is a control parameter, which may be multidimensional. Initially (t=0), the system is prepared in the ground state[1] of $H_{\lambda(t=0)}$, the initial Hamiltonian

$$\Psi(t{=}0) = \Psi^0_{\lambda(t=0)}. \tag{2}$$

From $t=0$ to $t=t_f$, the system undergoes an adiabatic evolution. We choose a path in parameter space, such that the ground state Ψ^0_λ of H_λ is non-degenerate at each point, so that it can be

[1] In all generality, the Berry phase is defined for any non-degenerate eigenstate. We use the ground state to simplify notation, but the generalization is straightforward.

differentiated along this path.[2] The adiabatic theorem states that for an adiabatic evolution, the system must remain in the ground state of the Hamiltonian H_λ at all times, which is defined up to an overall phase. In other words, at zeroth order of the adiabatic approximation

$$\Psi(t) = e^{i\phi(t)}\,\Psi^0_{\lambda(t)}. \tag{3}$$

Using this assumption, we can derive the value of $\phi(t)$ using the Schrödinger equation

$$i\hbar\frac{d|\Psi(t)\rangle}{dt} = H_{\lambda(t)}|\Psi(t)\rangle. \tag{4}$$

For practical reasons, we define $c^0(t) = e^{i\phi(t)}$. Inserting the adiabatic approximation into the Schrödinger equation, we obtain

$$i\hbar\dot{c^0}|\Psi^0_{\lambda(t)}\rangle + i\hbar c^0\,\frac{d|\Psi^0_{\lambda(t)}\rangle}{dt} = c^0 H_{\lambda(t)}|\Psi^0_{\lambda(t)}\rangle = c^0 E^0_{\lambda(t)}|\Psi^0_{\lambda(t)}\rangle, \tag{5}$$

where we have used the notation $\dot{c^0}$ for the time derivative of c^0, and $E^0_{\lambda(t)}$ is the lowest eigenvalue of $H_{\lambda(t)}$. This leads to the following differential equation for c^0

$$\dot{c^0} = c^0\left(-i\frac{E^0_{\lambda(t)}}{\hbar} - \langle\Psi^0_{\lambda(t)}|\,\frac{d|\Psi^0_{\lambda(t)}\rangle}{dt}\right). \tag{6}$$

Upon integration, using the initial condition $c^0(t{=}0) = 1$, or $\Phi(t{=}0) = 0$, we find

$$\Phi(t_f) = -\frac{1}{\hbar}\int_0^{t_f} E^0_{\lambda(t)}\,dt + i\int_0^{t_f}\langle\Psi^0_{\lambda(t)}|\frac{d|\Psi^0_{\lambda(t)}\rangle}{dt}\,dt\,. \tag{7}$$

There are thus two contributions to the phase associated with an adiabatic evolution, which are the two terms in the above expression:

- $\Phi_{\text{dyn}} = -\frac{1}{\hbar}\int_0^{t_f} E^0_{\lambda(t)}\,dt$ is the dynamical phase. It depends on the eigenenergies of the Hamiltonian, and on the time it takes to go through the adiabatic evolution.
- $\Phi_{\text{Berry}} = i\int_0^{t_f}\langle\Psi^0_{\lambda(t)}|\frac{d|\Psi^0_{\lambda(t)}\rangle}{dt}\,dt$ is the geometric or Berry phase.

Note that the integrand in the expression of the Berry phase is purely imaginary, such that Φ_{Berry} is a real number – it is a phase, not a decay of the wave function. It can easily be seen by noting that $\frac{d}{dt}\langle\Psi^0_{\lambda(t)}|\Psi^0_{\lambda(t)}\rangle = 0$ due to the normalization of the wavefunction.
During an adiabatic evolution, the wavefunction of a quantum system thus acquires a phase, the Berry phase, which only depends on the eigenstates visited by the evolution. It is important to note that the Berry phase is actually independent of time: it does not depend on how long it takes to go through the adiabatic path (assuming adiabaticity is preserved, of course). Indeed,

[2] We are defining here the abelian Berry phase. In case of a degenerate manifold, one can define a non-abelian Berry phase, as long as the manifold itself is separated by a gap from other states.

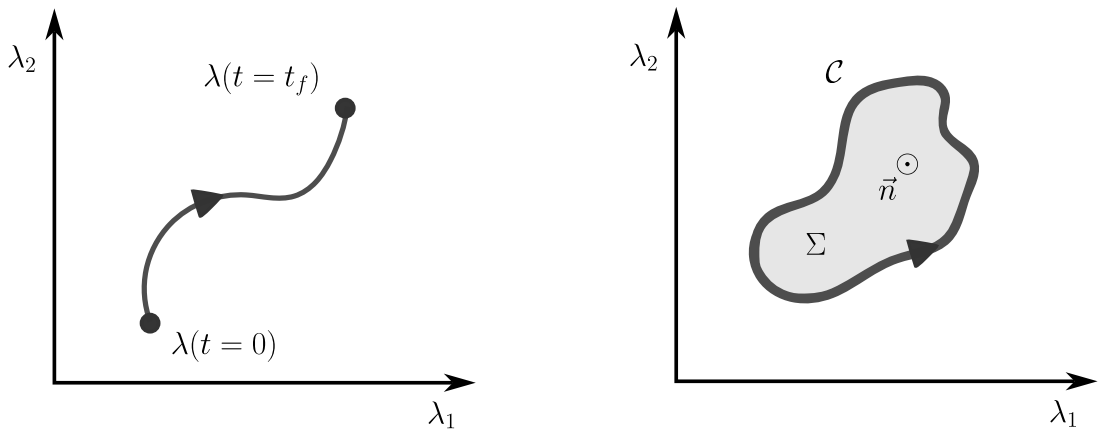

Fig. 2: *Open (left) and closed (right) paths in the multidimensional parameter space λ. We have used a two-dimensional parameter space for ease of representation.*

time can be removed from the expression of the Berry phase, by replacing the integral over time by an integral over the path in parameter space

$$\Phi_{\text{Berry}} = i\int_0^{t_f} \frac{d\lambda}{dt}\,\langle \Psi^0_{\lambda(t)}|\nabla_\lambda|\Psi^0_{\lambda(t)}\rangle\, dt = i\int_{\lambda(0)}^{\lambda(t_f)} \langle \Psi^0_\lambda|\nabla_\lambda|\Psi^0_\lambda\rangle\cdot d\lambda, \tag{8}$$

where we have used the notation $\nabla_\lambda = \left(\frac{\partial}{\partial\lambda_1}, \frac{\partial}{\partial\lambda_2}, \ldots\right)$ to express the gradient of the multidimensional variable λ.

2.2 Gauge invariance, Berry connection and Berry curvature

We start by defining the Berry connection (or Berry potential) $\mathcal{A}_\lambda$ as the real-valued vector field defined at every point on the parameter path, which, once integrated, is equal to the Berry phase

$$\mathcal{A}_\lambda = i\langle \Psi^0_\lambda|\nabla_\lambda|\Psi^0_\lambda\rangle. \tag{9}$$

The Berry connection is a gauge dependent quantity. Under a $U(1)$ gauge transformation of the wave function $\Psi^0_\lambda \to e^{i\chi_\lambda}\Psi^0_\lambda$, it transforms as

$$\mathcal{A}_\lambda \to \mathcal{A}_\lambda - \nabla\chi_\lambda. \tag{10}$$

For a generic path, the Berry phase is gauge dependent as well, and transforms as

$$\Phi_{\text{Berry}} \to \Phi_{\text{Berry}} + \chi_{\lambda(0)} - \chi_{\lambda(t_f)} \tag{11}$$

On the other hand, if the Berry phase is calculated along a closed path, it is clearly gauge independent. We define the notations for the contour $\mathcal{C}$, the enclosed surface Σ, and the unit vector $\vec{n}$ perpendicular to the surface in the right hand side of Fig. 2. If $\mathcal{A}_\lambda$ has no singularity within the contour, and the surface Σ is orientable, the contour integral in the expression of the Berry phase may be replaced by a surface integral of the flux of the curl of $\mathcal{A}_\lambda$ inside the contour, using Stokes' theorem

$$\Phi_{\text{Berry}} = \oint_{\mathcal{C}} \mathcal{A}_\lambda\cdot d\lambda = \iint_\Sigma (\nabla_\lambda \wedge \mathcal{A}_\lambda)\cdot\vec{n}\, d\sigma. \tag{12}$$

It is convenient, and customary, to define the Berry curvature, as the amplitude of the curl of the Berry connection

$$\Omega_\lambda = (\nabla_\lambda \wedge \mathcal{A}_\lambda) \cdot \vec{n}_z. \tag{13}$$

The Berry curvature is explicitly gauge independent, since the curl of a gradient is 0. If the manifold over which the Berry curvature is defined is compact, its integral over this entire manifold is an integer topological invariant called the Chern number.

2.3 Analogy to electromagnetism

The Berry curvature, Berry connection, and Berry phase, as defined in the previous paragraph, are reminiscent of similar concepts in the physics of electromagnetism. The gauge independent Berry curvature Ω_λ is analogous to a magnetic field, while the gauge dependent Berry connection corresponds to the vector potential $\vec{A}(\vec{r})$, whose curl is equal to the magnetic field. Additionally, a particle of charge q in a magnetic field undergoes the Aharonov-Bohm effect: upon traveling along a path $\mathcal{C}$, it acquires a Berry phase Φ_{AB}, which is called an Aharonov-Bohm phase and has the following expression

$$\Phi_{\mathrm{AB}} = \frac{q}{\hbar} \int_{\mathcal{C}} \vec{A}(\vec{r}) \cdot d\vec{r} = \frac{2\pi}{\Phi_0} \int_{\mathcal{C}} \vec{A}(\vec{r}) \cdot d\vec{r}, \tag{14}$$

where Φ_0 is a unit quantum of magnetic flux. For a closed loop, the Aharonov-Bohm phase is gauge independent, and is equal to the flux of the magnetic field through the loop.

3 Chern number in a condensed matter system

With the concepts of Berry curvature, Berry connection, and Berry phase defined in the previous section, we are now equipped to define the Chern number in the context of a condensed matter system. In this context, the Chern number characterizes the way the single-particle wave functions of a system change under variations of momentum. We will define it, explain why it must be an integer, and highlight its connection to the Hall conductance.

3.1 Bloch states and Chern number

In the previous section, we have used a generic parameter space λ; we will now focus on a two-dimensional space with discrete translation symmetry, such that the momentum along either space direction k_x and k_y is preserved, and defined in a compact space, the Brillouin zone. This is the familiar situation of a two-dimensional lattice system with periodic boundary conditions, and $(k_x, k_y) \in [-\pi/a, \pi/a]^2$, where a is the lattice constant.

In a system with discrete translation invariance, Bloch's theorem states that single-particle states may be expressed as the product of a plane wave $e^{i\vec{k}\cdot\vec{r}}$ and a periodic function $u_{\vec{k}}(r)$, called a Bloch state. We further assume a quantum system described by band theory, with a well isolated band. Note that in principle, one may calculate the Chern number of a group of bands, through

the non-abelian Berry connection, as long as this group is well isolated energetically from other bands. Here, we consider the Chern number of a single band, for simplicity. This condition is to ensure that single-particle eigenstates remain non-degenerate across the Brillouin zone. We can now define the Berry connection and Berry curvature associated with variations of momentum in terms of the Bloch states of said band

$$\mathcal{A}^{x,y}_{\vec{k}} = i\langle u_{\vec{k}}|\partial_{k_{x,y}} u_{\vec{k}}\rangle \tag{15}$$

$$\Omega_{\vec{k}} \;\; = \partial_{k_x}\mathcal{A}^{y}_{\vec{k}} - \partial_{k_y}\mathcal{A}^{x}_{\vec{k}}. \tag{16}$$

The Chern number of the band is defined as the integral of the Berry curvature over the Brillouin zone

$$C = \frac{1}{2\pi}\int_{BZ} \Omega_{\vec{k}}\, dk_x dk_y. \tag{17}$$

3.2 Chern number without translation invariance

Let us comment on the assumption of translational invariance: it is a convenient assumption, which allows us to use k_x and k_y, but not a necessary one. For a system without translational invariance (such as a system with edges, or disorder, or an amorphous lattice), one may define a local Chern marker [9]

$$C_{xy}(\mathbf{r}) = -2\pi i \,\mathrm{Tr}\left[Q\hat{x}, P\hat{y}\right], \tag{18}$$

where $\hat{x}, \hat{y}$ are position operators, and P, $Q{=}\mathbb{1}{-}P$ are projectors onto occupied and unoccupied states. The local Chern marker may not be quantized, but its average in the bulk of an insulator is.

3.3 Many-body Chern number

The second assumption we made was that of a system described by band theory, such that the approximation of independent electrons can be used, and the Chern number may be calculated from single-particle states. More generally, one may define the many-body Chern number of a correlated insulator, based on its many-body wavefunction Ψ_{MB} [10]. The parameter space over which the evolution of Ψ_{MB} is examined is that of the twist angles θ_x, θ_y of periodic boundary conditions, i.e., the wavefunctions satisfy $\phi(x, y{=}L_y) = e^{i\theta_y}\,\phi(x, y{=}0)$ and $\phi(x{=}L_x, y) = e^{i\theta_x}\,\phi(x{=}0, y)$. For a non-degenerate insulator, which remains non-degenerate at all twist angles, the many-body Berry connection writes

$$\mathcal{A}^{x,y}_{\vec{\theta}} = \langle \Psi_{MB}|\partial_{\theta_{x,y}}\Psi_{MB}\rangle. \tag{19}$$

The many-body Berry curvature and Chern number are then defined very similarly to their band theory counterparts. The many-body Berry curvature writes

$$\Omega^{MB}_{\vec{\theta}} = \partial_{\theta_x}\mathcal{A}^{y}_{\vec{\theta}} - \partial_{\theta_y}\mathcal{A}^{x}_{\vec{\theta}} \tag{20}$$

and integration over the twist angles yields the many-body Chern number

$$C^{MB} = \frac{1}{2\pi}\iint \Omega^{MB}_{\vec{\theta}} \tag{21}$$

Note that for large enough systems, the integral over the twist angle may be omitted, and the many-body Chern number may be evaluated from the many-body Berry curvature at any angle, as self-averaging occurs within the many-body wave function in the thermodynamic limit [11].

3.4 Explicitly gauge invariant expression of the Chern number

The Chern number, as expressed in Eq. (17) is clearly gauge invariant, as the integral of the Berry curvature, even though the Bloch states are not. It is convenient to introduce an expression of the Chern number, which is explicitly gauge invariant [12]. This is especially practical when calculating the Chern number in a concrete model: it fixes any gauge discrepancy introduced by the determination of Bloch states through numerical diagonalization without having to introduce a smooth gauge explicitly.

To obtain the gauge invariant expression of the Chern number, we will decompose it into the sum of Berry phases associated with the change of momentum when going around the infinitesimal square loop $l_{\vec{k}}$

$$l_{\vec{k}} : \vec{k} \to \vec{k}+d\vec{k}_x \to \vec{k}+d\vec{k}_x+d\vec{k}_y \to \vec{k}+d\vec{k}_y \to \vec{k}. \tag{22}$$

In terms of the Bloch states, this Berry phase may be written as

$$\begin{aligned}\gamma_{\vec{k}} &= \oint_{l_{\vec{k}}} \mathcal{A}\cdot d\vec{l} \\ &= idk_x\langle u_{\vec{k}}|\partial_{k_x}u_{\vec{k}}\rangle + idk_y\langle u_{\vec{k}+d\vec{k}_x}|\partial_{k_y}u_{\vec{k}+d\vec{k}_x}\rangle \\ &\quad - idk_x\langle u_{\vec{k}+d\vec{k}_x+d\vec{k}_y}|\partial_{k_x}u_{\vec{k}+d\vec{k}_x+d\vec{k}_y}\rangle - idk_y\langle u_{\vec{k}+d\vec{k}_y}|\partial_{k_y}u_{\vec{k}+d\vec{k}_y}\rangle.\end{aligned} \tag{23}$$

Using the following identity (first order expansion of the exponential)

$$idt\langle u|\frac{d}{dt}u\rangle = -\operatorname{Im}\log\big\langle u(t)\big|u(t+dt)\big\rangle + \mathcal{O}(dt^2) \tag{24}$$

the infinitesimal Berry phase is expressed as an overlap of Bloch wavefunctions, which is explicitly gauge invariant

$$\gamma_{\vec{k}} = -\operatorname{Im}\log\langle u_{\vec{k}}|u_{\vec{k}+d\vec{k}_x}\rangle\langle u_{\vec{k}+d\vec{k}_x}|u_{\vec{k}+d\vec{k}_x+d\vec{k}_y}\rangle\langle u_{\vec{k}+d\vec{k}_x+d\vec{k}_y}|u_{\vec{k}+d\vec{k}_y}\rangle\langle u_{\vec{k}+d\vec{k}_y}|u_{\vec{k}}\rangle. \tag{25}$$

The Chern number may thus be evaluated through an explicitly gauge invariant product of overlaps of Bloch states, as

$$C = \frac{1}{2\pi}\int_{BZ}\gamma_{\vec{k}}\, dk_x dk_y. \tag{26}$$

3.5 Chern number and Hall conductance

The remarkable discovery by Thouless, Khomoto, Nightingale, den Nijs (TKNN) [13] was to connect the Hall or transverse conductance of insulators to the Chern number

$$\sigma_{xy} = \frac{e^2}{h} \sum_{i \in \text{occupied}} C_i \tag{27}$$

In units of the quantum of conductance e^2/h, the transverse conductance is given by the sum of the Chern numbers of all occupied bands. Because of this discovery, the Chern number in the context of condensed matter is sometimes called the TKNN integer.
The goal of TKNN was to explain the quantization of σ_{xy} in the integer quantum Hall effect (so far explained through Laughlin's charge pumping argument, as we will explain later), by connecting it mathematically to a quantized quantity. To do so, they introduced a periodic potential, and calculated σ_{xy} within linear response through the Kubo formula, yielding the Chern number. As already mentioned in the first section of these lecture notes, this relationship between the Hall conductance of insulators and the Chern number explains the remarkable accuracy (metrologically precise) of the quantization of σ_{xy}, regardless of the specific details of the disorder landscape in the sample.

3.6 The Chern number is an integer

Here, we expose two arguments explaining why the Hall conductance of insulators must be quantized. The first one is Laughlin's historical argument for the quantization of σ_{xy} in the integer quantum Hall effect. The second one is a more mathematical argument, based on the definition of different gauges throughout the Brillouin zone to calculate the Chern number.

3.6.1 Laughlin's argument: the charge pump

Soon after the experimental discovery of the integer quantum Hall effect, Laughlin proposed the first explanation of the quantization of the Hall conductance [14]. Laughlin's argument is based on a topological charge pump, and applies to any system with vanishing longitudinal conductance (any insulator). We summarize it here in simple terms.
Let us picture a sample in the cylinder geometry, i.e., a rectangle with periodic boundary conditions along the y direction (see Fig. 3). Threading a magnetic flux along the cylinder axis does not change the overall magnetic field going through the sample (no additional Hall effect). However, due to Faraday's law of induction, such magnetic flux creates a current along the x direction, from one edge of the cylinder to the other. For an adiabatic flux insertion, this current may be approximated as the adiabatic derivative of the energy with respect to the inserted flux

$$J = c \frac{\partial E_\Phi}{\partial \Phi} \,. \tag{28}$$

For a large enough cylinder perimeter, Aharonov-Bohm oscillations are suppressed, and we can replace the derivative by a finite difference

$$J = c \frac{\Delta E}{\Delta \Phi} \,. \tag{29}$$

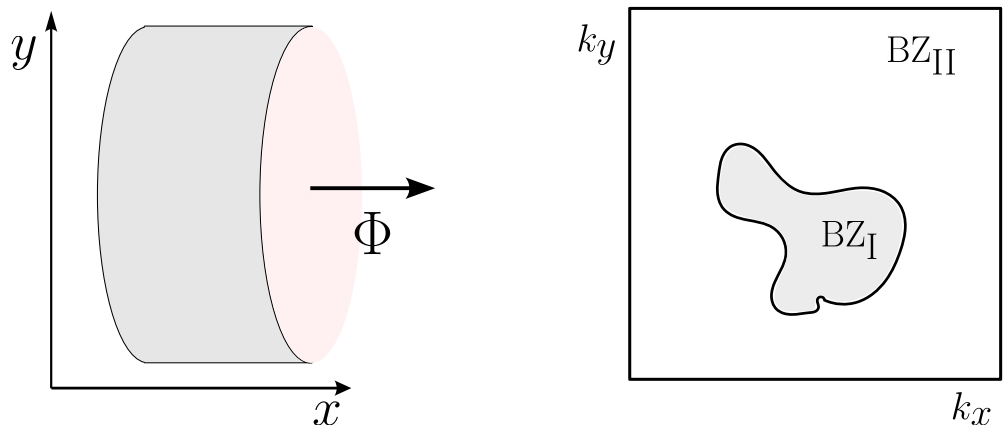

Fig. 3: *Arguments for the quantization of σ_{xy} and C. (Left) Laughlin charge pump. As a quantum of magnetic flux is adiabatically inserted along the axis of a cylinder, an integer number of electrons is transferred from one edge to the other. (Right) When the Chern number is $C \neq 0$, it is impossible to define a smooth gauge over the whole Brillouin zone. We define at least two regions I and II, and the Chern number may be calculated from the singularity of wave functions at their boundary.*

We consider the insertion of a quantum of flux $\Phi_0 = hc/e$. After the insertion, the Hamiltonian must go back to its initial form up to a gauge transform, such that all energy levels remain the same. The difference of energy thus originates only from the difference of occupation of these states, i.e., the transfer of n electrons from one edge to the other, where p is an integer, which results in a difference of potential V between both edges. The Hall conductance (for vanishing longitudinal conductance) then writes

$$\sigma_{xy} = \frac{J}{V} = pc\,\frac{e}{\Phi_0} = n\,\frac{e^2}{h}\,. \tag{30}$$

As expected, we find that the Hall conductance is quantized, and equal to an integer in units of the quantum of conductance.

3.6.2 The Chern number as an obstruction to the definition of a smooth gauge for Bloch states

There are several ways to gain an intuitive understanding of what is the Chern number. Here, we will explain one such possible interpretation: when the Chern number is non-zero, there must be some gauge discontinuity for the Bloch states – in other words, it is not possible to use the same gauge definition throughout the Brillouin zone.
Let us first reason by contradiction, and assume that there exists a smooth gauge throughout the entire Brillouin zone. The gauge defined for the Bloch states also applies to the Berry connection, such that we may use Stokes' theorem to express the Chern number as an integral of the Berry connection over the surface boundary $\mathcal{C}$. The surface being the Brillouin zone, it does not have a boundary: the contour $\mathcal{C}$ is reduced to a point, and the Chern number is 0.

$$C = \frac{1}{2\pi}\int_{BZ} \Omega_{\vec{k}}\, dk_x dk_y = \oint_{\mathcal{C}} \mathcal{A}\cdot dl = 0. \tag{31}$$

To gain further insight, let us take the example of a generic two-band model, such that there are two sites A and B per unit cell. The Bloch states are 2-dimensional spinors parametrized by the complex numbers α_k and β_k

$$|u_k\rangle = \alpha_k|A_k\rangle + \beta_k|B_k\rangle. \tag{32}$$

A possible gauge choice, which we call gauge I, is to fix that α_k is a real positive number, which is a valid gauge choice, as long as $\alpha_k \neq 0$. If $\alpha_k = 0$, we need a different gauge; we choose gauge II such that β_k is a real positive number. Since α_k and β_k cannot vanish at the same time, we can always choose one gauge or the other, and we can divide the Brillouin zone into two zones, one with gauge I ($\mathrm{BZ_I}$), one with gauge II ($\mathrm{BZ_{II}}$). See Fig. 3.
On the boundary between the two zones $\mathrm{BZ_I}$ and $\mathrm{BZ_{II}}$, $\alpha_k \neq 0$ and $\beta_k \neq 0$, and the Bloch states and Berry connection are related by the following gauge transform

$$|u_k\rangle_{\mathrm{I}} = e^{i\chi(k)}|u_k\rangle_{\mathrm{II}} \tag{33}$$

$$\mathcal{A}_{\mathrm{I}} = \mathcal{A}_{\mathrm{II}} + \nabla\chi(k). \tag{34}$$

We are now equipped to calculate the Chern number, by using Stokes' theorem separately in $\mathrm{BZ_I}$ and $\mathrm{BZ_{II}}$. $\mathcal{B}$ denotes the oriented boundary between these two zones, which may be continuous or made of several parts.

$$C = \frac{1}{2\pi}\int_{\mathrm{BZ_I}} \omega_k \, dk_x dk_y + \frac{1}{2\pi}\int_{\mathrm{BZ_{II}}} \omega_k \, dk_x dk_y = \frac{1}{2\pi}\oint_{\mathcal{B}} (\mathcal{A}_{\mathrm{I}} - \mathcal{A}_{\mathrm{II}}) \cdot dl = \frac{1}{2\pi}\oint_{\mathcal{B}} \nabla\chi(k) \cdot dl \tag{35}$$

The last contour integral evaluates to $\chi(k^*_+) - \chi(k^*_-)$, where k^* is any chosen point on the contour, and the index $\pm$ corresponding to its limits when approaching from either side on the contour. It must be equal to $2\pi n$, where n is an integer, since the Bloch state $|u^*_k\rangle$ is single valued. As a result

$$C = n \tag{36}$$

and the Chern number is an integer, which accounts for the gauge discontinuities within the Brillouin zone.

3.7 Edge states

Shortly after Laughlin's explanation of the quantization of σ_{xy} in the quantum Hall effect through a charge pump [14], Halperin realized [15] that there must be a chiral mode conducting current at the edge of the system, and that this mode also explains the quantization. Halperin's argument may be generalized to all band insulators with a Chern number $C \neq 0$: there must be C one-dimensional chiral modes at the edge. It is an example of the bulk-boundary correspondence of topological insulators: the existence of a topological invariant in the bulk implies the existence of robust gapless modes at the edge. Here, we give a simple image for this argument, and highlight some consequences.
The crux of Laughlin's argument is that charges are being transferred adiabatically from one edge of the sample to the other following the insertion of a quantum of flux. This charge transfer

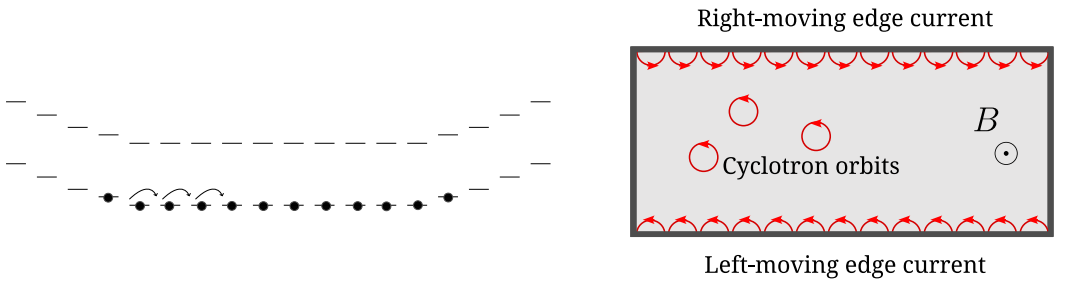

Fig. 4: *Chiral edge states in the quantum Hall effect. (Left) Effect of a confining potential on the Landau levels. The Fermi level crosses a Landau level where its group velocity is non-zero, hence the chirality of edge modes. During a Laughlin charge pump, transport occurs from one edge to the other because the inserted magnetic flux moves the Landau level states from one side to the other. (Right) Semi-classical picture of the chiral edge modes, with skipping orbits at the edge.*

implies the existence of a reservoir of charges (electrons or holes) at each edge. Moreover, the reservoirs must be gapless to ensure the adiabaticity of transport; therefore, there must be gapless edge modes in order to have $\sigma_{xy} \neq 0$.

In the quantum Hall effect, the chirality of edge modes is easily seen by considering the effect of a confining potential on the single-particle energy spectrum (see Fig. 4 left). Independent electrons in 2D in a magnetic field occupy degenerate energy levels called Landau levels, which are perfectly flat unless one introduces a confining potential. This confining potential creates a curve on either ends of the Landau levels, ensuring that the energy of electrons becomes infinite far away from the sample. Edge modes correspond to the crossing between the Fermi level and a curved Landau level: their chirality is given by the sign of the group velocity $\partial E/\partial r$ at the crossing.

The semiclassical picture of electrons in a magnetic field also provides an intuitive understanding of the origin of chiral edge modes (see Fig. 4 right). Due to the Lorentz force $-e\vec{v} \wedge \vec{B}$, electrons move in a circular fashion, with an orientation determined by the sign of the magnetic field. In the bulk of the sample, these orbits are closed, but the presence of the edge prevents the orbit from closing, forcing a pattern of skipping orbits, where the current only goes in one direction on one edge, and in the other direction on the opposite edge.

Whether in a quantum Hall system, or more generally in a Chern insulator, the edge modes are dissipationless, and protected against any local perturbation, particularly disorder. Because of their chirality, backscattering into the same channel is not allowed, and backscattering into the edge mode with the opposite chirality is exponentially suppressed by the presence of a gap in the bulk, as long as the edges are sufficiently far apart. We say that the gapless edge modes of Chern insulators are topologically protected. The existence of a dissipationless chiral mode would be impossible in a purely one-dimensional system, which is consistent with the fact that all 1D systems are Anderson localized for any disorder strength. Here, it is the presence of the 2D topological bulk, which makes it possible. One may also note that a Chern number C implies the existence of C dissipationless chiral edge modes, through the Landauer-Buttiker formalism. There could be more edge modes, but they would not be protected against disorder.

4 Chern insulator models

As we have explained in the previous section, a Chern insulator is a band insulator, such that the total Chern number of bands below the gap is non-zero. We have also defined the necessary concepts, and highlighted some very general consequences, such as a non-zero Hall conductance and the presence of robust chiral edge modes. To make things more concrete, we will now detail some explicit Chern insulator models. This will help us obtain an intuition of the microscopic ingredients that make topology possible in a model. We will provide some examples of their realizations, focusing on solid state and cold atom implementations. For a more complete review of topological phases of cold atoms, we refer to the J. Dalibard' lecture series [16].

4.1 Harper-Hofstadter model

In the previous sections, we have made many references to the quantum Hall effect, which arises for electrons confined to two dimensions in a transverse magnetic field. Our first model is a lattice version of the (continuum) quantum Hall effect, introduced by Harper in 1955 [17], and solved by Hofstadter in 1976 [18].

4.1.1 Minimal coupling to a magnetic field

We consider a tight-binding model of non-interacting particles hopping between neighboring sites of a square lattice

$$H = -\sum_{<i,j>} t\left(c_i^\dagger c_j + c_j^\dagger c_i\right) \tag{37}$$

If we add a magnetic field, the hopping amplitude on the lattice should acquire a phase equal to the Aharonov-Bohm phase associated with the coupling of a charged particle to the electromagnetic vector potential $\vec{A}$

$$-tc_i^\dagger c_j \rightarrow -t\, e^{i\frac{2\pi}{\Phi_0}\int_{r_i}^{r_j}\vec{A}(\vec{r})\cdot d\vec{r}}\, c_i^\dagger c_j, \tag{38}$$

where Φ_0 is a unit quantum of magnetic flux. To make the model more explicit, we choose the Landau gauge

$$\vec{A} = (0, Bx, 0). \tag{39}$$

Within this gauge choice, our tight-binding model has complex hopping amplitudes on the vertical bonds, with a phase $e^{i\Phi x}$, which ensures a total flux $\Phi = Ba^2$ through each minimal square plaquette, where a is the lattice constant (see Fig. 5).

The Hofstadter model is very rich, with an energy spectrum as a function of flux per lattice plaquette Φ, which has a fractal structure called the Hofstadter butterfly. For our purpose of introducing a topological model, we focus on the simpler case where Φ is a rational number p/q in units of the quantum of magnetic flux Φ_0. In this case, one notices that the Hofstadter model has an enlarged unit cell compared to the original square lattice with no magnetic field. Indeed, there is a translation symmetry by q lattice sites in the x direction, and by 1 lattice site in the

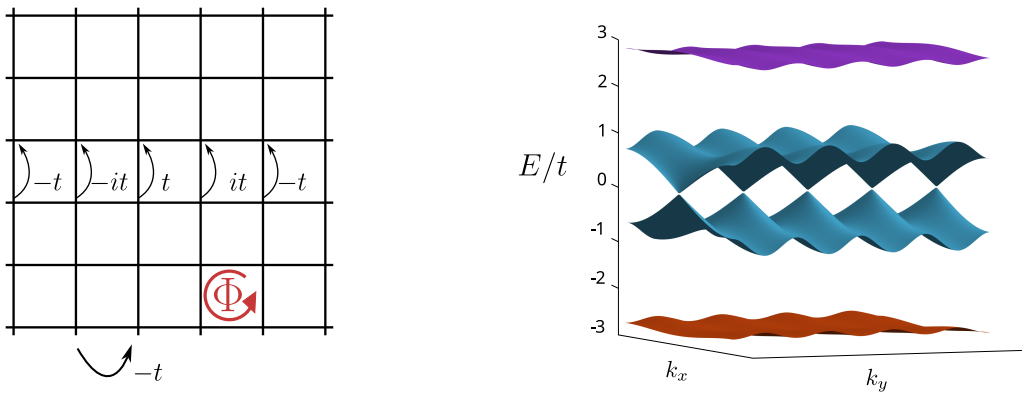

Fig. 5: *The Harper-Hofstadter model on a square lattice for a flux per plaquette $\Phi = \pi/2$. (Left) Sketch of the model: a square lattice with nearest-neighbor hopping of amplitude t on horizontal bonds, and $te^{i\Phi x}$ (respectively $te^{-i\Phi x}$) on upward (respectively downward) vertical bonds. (Right) Band structure of the Harper-Hofstadter model with flux $\pi/2$ per plaquette. The lowest band is well separated from other bands by a gap, and carries a Chern number 1.*

y direction. As a result, there are q bands in this model. The lowest band of the Hofstadter model carries a Chern number $C = 1$. Other bands also carry a non-zero Chern number, and the sum over all bands yields a total Chern number 0, as for any lattice model. We will not demonstrate this result, which may be obtained by applying the Chern number formula onto the Bloch wavefunctions of the lowest band of the model. Of course, this is not a surprising result: since we explicitly added a magnetic field in the model, we expect to recover the physics of the quantum Hall effect. In the continuum limit $\Phi \ll \Phi_0$, the bands are the non-dispersive Landau levels of the quantum Hall effect. For larger Φ, lattice effects are more important, and the bands carry some dispersion.

4.1.2 Physical relevance of the Hofstadter model – solid state

In typical crystalline solids, such as graphene, or the semiconductor quantum wells typically used in quantum Hall experiments, lattice effects are irrelevant, and a continuum model is perfectly sufficient. Indeed, for a lattice unit cell with a size of a few Ångström, it would take a magnetic field of 10^5 Tesla to achieve a unit quantum of flux Φ_0 per unit cell, which is several orders of magnitude beyond current possibilities.

Lattice effects may become more important in solid state systems if the unit cell is significantly enlarged, for example by creating a moiré superlattice (see Fig. 6). By stacking two atomically thin two-dimensional materials with a slight lattice constant mismatch, or two or more layers of the same 2D material with a small angle misalignment, one obtains an interference pattern of the two lattices, with a much larger periodicity than the original lattices. In these moiré heterostructures, the superlattice scale can be of order 10 nm, which allows the emergence of Hofstadter physics at accessible magnetic fields of the order of 10 Tesla. This effect was first well demonstrated in an experiment [19] where a (well aligned, or Bernal stacked) bilayer of graphene was stacked on top of a substrate of hexagonal boron nitride, a two-dimensional

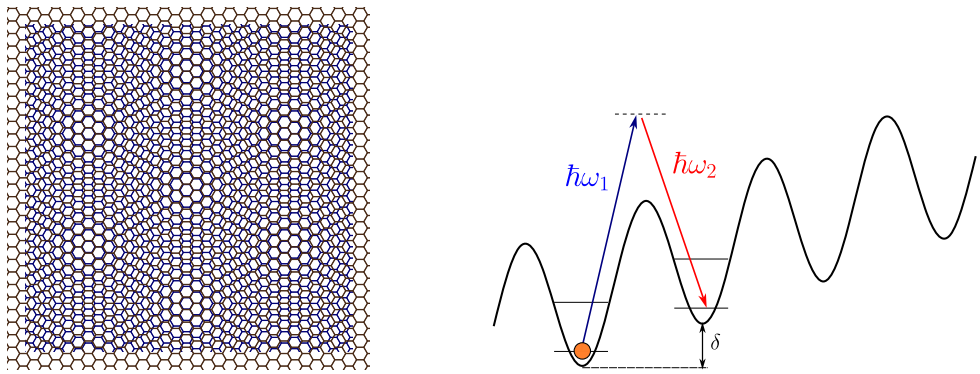

Fig. 6: *Implementation of the Harper-Hofstadter model in solid state (left) and cold atoms in optical lattices (right). (Left) Moiré superlattice resulting from the alignment of a graphene and an hexagonal boron nitride (hBN) layer, which have a* 10% *lattice constant mismatch. There, a sizable fraction of a magnetic flux per superlattice triangular plaquette is achievable with magnetic fields of 1–10 Tesla. (Right) Laser-assisted tunneling in an optical lattice: an atom in the ground state of a given lattice site is excited to a high energy state, followed by stimulated emission to the ground state of the neighboring site. Through this process, a complex factor* $e^i(k_1-k_2)\cdot r$ *is imprinted onto its wave function, achieving the desired Aharonov-Bohm phase.*

insulator with a lattice constant very close to that of graphene. The Harper-Hofstadter model, with the square lattice replaced by a triangular lattice to fit the crystal structure of these two-dimensional solids, then describes very well the physics of moiré systems under a magnetic field.

4.1.3 Realization of the Harper-Hofstadter model in cold atoms

Tight-binding models are realized in ultracold atomic gases by using an optical lattice, i.e., an array of standing waves, which create a periodic potential for the neutral atoms. Such a set-up provides the original hopping model, without any complex amplitude corresponding to the Aharonov-Bohm effect. To simulate the effect of the magnetic field on the neutral atoms, Jaksch and Zoller [20] proposed a method of Raman-assisted tunneling, which imprints the Aharonov-Bohm phase onto specified tunneling terms, and realizes the Harper-Hofstadter model.

The basic idea of laser-assisted tunneling is summarized in Fig. 6. To imprint an artificial gauge field onto the optical lattice, one first needs to inhibit the direct (real amplitude) transition. Using the gauge choice defined in Eq. (39), we leave the periodic potential unaffected in the x direction, and inhibit transitions along the vertical bonds by detuning the potential through an energy mismatch δ between neighboring sites. The tunneling is then restored by adding two Raman lasers at resonance with this mismatch: $\delta = \hbar\omega_1 - \hbar\omega_2$. To tunnel, an atom thus follows a two-step process, summarized in Fig. 6: absorption of a photon of frequency ω_1, followed by the stimulated emission of a photon of frequency ω_2. The tunneling occurs with a phase, which corresponds to the wavevector mismatch between the two lasers: $e^{i(\vec{k_1}-\vec{k_2})\cdot\vec{r}}$. This method was implemented by two independent groups in 2013, with flux per plaquette $\Phi/\Phi_0 = \pi/2$ [21] and π [22], respectively.

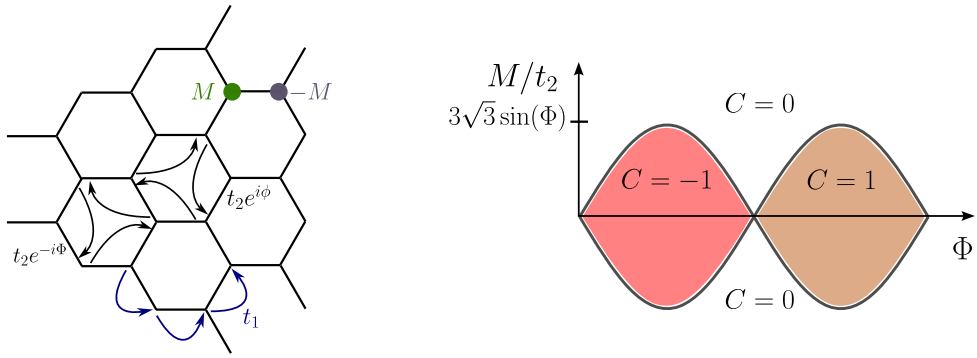

Fig. 7: *Haldane model of a Chern insulator [23]. (Left) The model consists of a honeycomb lattice with nearest-neighbor hopping of real amplitude t_1, second-neighbor hopping of amplitude $t_2e^{i\Phi}$, and a staggered on-site mass M for sites A and B. (Right) Phase diagram of the Haldane model. Depending on the values of the parameter M/t_2, the lowest band has Chern number 0, 1, or -1. The Chern number is opposite in the other band.*

4.2 Haldane model

The Harper-Hofstadter model described in the previous section is simply a lattice model in a magnetic field. In 1988, Haldane [23] realized that there is no need for a net field to obtain a non-zero Chern number, and hence a quantized Hall effect. He developed a model based on a hexagonal lattice, with a staggered flux, such that the overall magnetic flux per unit cell is zero. Beyond the absence of a magnetic field, Haldane showed that there are distinct ways to open a gap in a gapless system, which respectively result in trivial or topological bands. We now go into the details of the model and its different terms, and discuss its relevance to solid state systems, and its implementation in cold atoms in optical lattices. Fig. 7 summarizes the model.

4.2.1 Graphene tight-binding model, and different gap opening terms

We start from graphene's tight-binding model, which consists of nearest-neighbor hopping on a honeycomb lattice. There are two inequivalent lattice sites A and B, thus we can write the Hamiltonian in the following form

$$H = -t_1 \sum_i c_A^\dagger(\vec{r}_i)c_B(\vec{r}_i) + c_A^\dagger(\vec{r}_i)c_B(\vec{r}_i+\vec{a}_1) + c_A^\dagger(\vec{r}_i)c_B(\vec{r}_i+\vec{a}_2) + h.c. \tag{40}$$

where $\vec{a_1}$ and $\vec{a_2}$ are the Bravais lattice vectors of the triangular lattice. Going into momentum space, one may rewrite the Hamiltonian in Bloch form

$$H = \sum_{\vec{k}} \begin{pmatrix} A_{\vec{k}} & B_{\vec{k}} \end{pmatrix} h\left(\vec{k}\right) \begin{pmatrix} A_{\vec{k}} \\ B_{\vec{k}} \end{pmatrix}. \tag{41}$$

where the Bloch Hamiltonian is a 2×2 matrix, and writes

$$h\left(\vec{k}\right) = -t_1 \begin{pmatrix} 0 & 1+e^{-i\vec{k}\cdot\vec{a_1}}+e^{-i\vec{k}\cdot\vec{a_2}} \\ 1+e^{i\vec{k}\cdot\vec{a_1}}+e^{i\vec{k}\cdot\vec{a_2}} & 0 \end{pmatrix}. \tag{42}$$

Diagonalizing this Hamiltonian yields the two energy bands of graphene

$$E_{\pm}\big(\vec{k}\big) = \pm t_1 \sqrt{\Big(1+\cos\big(\vec{k}\cdot\vec{a_1}\big)+\cos\big(\vec{k}\cdot\vec{a_2}\big)\Big)^2 + \Big(\sin\big(\vec{k}\cdot\vec{a_1}\big)+\sin\big(\vec{k}\cdot\vec{a_2}\big)\Big)^2}. \tag{43}$$

The two bands touch at the two inequivalent corners of the hexagonal Brillouin zone, $\vec{K^{\pm}}$. In the vicinity of these points, the dispersion relation is linear, describing relativistic particles, and the Hamiltonian takes the Dirac form

$$h\big(q=\vec{k}-\vec{K^{\pm}}\big) = \frac{3}{2} t_1 a\big(\pm q_x\sigma_x + q_y\sigma_y\big) \tag{44}$$

where σ_x, σ_y, σ_z are the Pauli matrices.

The Dirac crossings in the honeycomb lattice model are protected by the product of two symmetry operators, inversion $\mathcal{C}_2$ and time-reversal symmetry $\mathcal{T}$. This means that no gap opening can occur, as long as these symmetries are preserved. Let us examine the effect of a gap opening via breaking of $\mathcal{C}_2$ symmetry. This can be done by introducing an on-site mass term, which gives a different energy to sites A and B. The extra term in the Bloch Hamiltonian writes

$$M\sigma_z \tag{45}$$

and the new energy spectrum is

$$E_{\pm}\big(\vec{k}\big) = \sqrt{M^2 \pm t_1^2\left(\Big(1+\cos\big(\vec{k}\cdot\vec{a_1}\big)+\cos\big(\vec{k}\cdot\vec{a_2}\big)\Big)^2 + \Big(\sin\big(\vec{k}\cdot\vec{a_1}\big)+\sin\big(\vec{k}\cdot\vec{a_2}\big)\Big)^2\right)} \tag{46}$$

For this new band structure, the only gap closing occurs at $M=0$. Note that taking the limit $M \to \pm\infty$ yields two decoupled copies of a triangular model with one site per unit cell. Such a model is necessarily topologically trivial, since there is only one band.[3] As a result, adding a staggered mass in the Haldane model results in two topologically trivial $C=0$ bands.

We now add a different term to the honeycomb lattice model, in the form of a next-nearest-neighbor hopping of amplitude $t_2 e^{i\Phi}$ (see Fig. 7). This term breaks time-reversal symmetry, since a time-reversal conjugation transforms $e^{i\Phi}$ into $e^{-i\Phi}$, but unlike the Harper-Hofstadter model, the unit cell is unchanged, and the total flux per hexagon is zero. This adds a diagonal term to the Bloch Hamiltonian, of the form

$$2t_2\sin(\Phi)\big(-\sin(ka_1)+\sin(ka_2)-\sin(ka_1{+}ka_2)\big)\,\sigma_z \tag{47}$$

$$+2t_2\cos(\Phi)\big(\ \ \cos(ka_1)+\cos(ka_2)+\cos(ka_1{+}ka_2)\big)\mathbb{1} \tag{48}$$

This term also opens a gap in the spectrum of the graphene model, but unlike the mass term, it has opposite signs at the K^+ and K^- points. This allows the bands to acquire a non-zero Chern number whenever the time-reversal breaking term dominates over the mass term, i.e., $|M/t_2| < 3\sqrt{3}\sin\Phi$, as can be verified through a direct calculation of the Chern number. See Fig. 7 for a phase diagram of the lowest band of the Haldane model.

[3] To convince ourselves that a one band model necessarily has Chern number 0, one can recall the obstruction to defining a smooth gauge in the entire Brillouin zone: the one-dimensional wavefunction cannot vanish anywhere in the entire Brillouin zone because it must remain normalized.

4.2.2 Physical relevance of the Haldane model in the solid state – spin-orbit coupling

In a seminal paper [3], Kane and Mele demonstrated that the phase-carrying hopping terms of the Haldane model could actually be physically relevant to graphene, when introducing the appropriate spin-orbit coupling term. Yet, graphene preserves time-reversal symmetry, and the Haldane model does not. This issue is resolved by taking two time-reversed copies of the graphene's honeycomb model, one for each spin. Kane and Mele showed that spin-orbit coupling introduces a complex tunneling next-nearest neighbor term, with opposite phases for each spin, such that time-reversal symmetry is preserved. This realizes a model for what is known as the quantum spin Hall effect, a topological insulator, which can be thought of as a product of two Chern insulators with opposite Chern numbers. It turns out that the actual spin-orbit coupling term is much too weak to produce a measurable gap in graphene, and that physical realizations of topology have to be searched for elsewhere.
The first quantum spin Hall insulator was realized in quantum wells of HgTe / HgCdTe [24]. However, no time-reversal symmetry breaking (or spin polarization) was achieved there. The first Chern insulator was realized [25–27] in thin films of three-dimensional topological insulators, doped with a magnetic element, follwing a theoretical prediction [28]. The 3D topological insulators (e.g. $(Bi,Sb)_2Te_3$) are materials with a large spin-orbit coupling, which plays the role of creating non-trivial topology in the band structure. The magnetic doping element (e.g. Cr or Fe) breaks time-reversal symmetry, by allowing the spin polarization of the ground state.

4.2.3 Realization of the Haldane model in cold atoms

The Haldane model was realized using ultracold fermions in an optical lattice [29]. The time-reversal breaking next-nearest neighbor hopping terms are implemented through a circular modulation of the lattice positions, i.e., by 'shaking' the lattice in a circular motion. Similarly to the laser-assisted tunneling process described in the realization of the Harper-Hofstadter model, the periodic modulation of the lattice may be treated using Floquet theory, in order to obtain the effective Hamiltonian, which is here the Haldane model.

4.3 Chern number and spontaneous symmetry breaking in moiré materials

The latest observations of a solid state Chern insulator occurred in two-dimensional moiré materials, namely twisted bilayer graphene aligned with hexagonal boron nitride [30], twisted bilayer transition metal dichalcogenites (MoTe2) [31], as well as other graphene systems aligned with hexagonal boron nitride. In these materials, time-reversal symmetry is broken spontaneously, and not explicitly, as a result of strong interactions, while the topology has a different origin depending on the specific moiré material.
Integer quantum Hall states at integer filling are spin polarized. While this makes sense from the point of view of single-particle physics, since the Zeeman interaction lifts the degeneracy between spin up and down within a Landau level, the main contribution to this ferromagnetism

comes from electronic interactions. Essentially, a spin-polarized wavefunction must be spatially antisymmetric, which lowers its Coulomb interaction compared to other wavefunctions, through a process called exchange. A similar process can occur in any flat band, i.e., a band with a low enough dispersion, such that interactions dominate over kinetic energy, as long as the single-particle states of the flat band have a sufficient overlap with one another (i.e. the flat band is the result of a quantum interference between different states, rather than orbitals localized on individual sites). Moiré materials are an example of such material, where the band can be flattened, for example by tuning the rotation angle between two layers to a 'magic angle' condition.

Twisted bilayer graphene consists of two layers of graphene, misaligned with an angle θ. A superlattice (or moiré) potential results from this misalignment, which folds the bands of graphene onto themselves, inside a mini Brillouin zone. At each band crossing (resulting either from this folding, or from two bands from two different layers), there is a gap opening due to level repulsion and interlayer tunneling. If we focus around the middle of the spectrum, which is relevant at low energy because this is typically where the Fermi energy lies, there are the Dirac cones originating from each graphene layer. Similarly to graphene, the Dirac cones are protected by the product of inversion $\mathcal{C}_2$ and time-reversal symmetry $\mathcal{T}$. Similarly to our discussion of the Haldane model, this gives us different ways to open a gap. Yet, twisted bilayer graphene presents a very important difference compared to graphene: the chirality of the Dirac cones is the same at opposite corners of the Brillouin zones for a given valley, with the other valley restoring time-reversal symmetry by having the opposite chirality. In contrast, the chirality of the Dirac cones is opposite for the opposite corners of the Brillouin zone in graphene. This peculiar configuration, which is only observed through the interference of two graphene layers, leads to the fact that a simple staggered mass term (equivalent to that of the Haldane model) may in fact open a topological gap in twisted bilayer graphene's band structure [32], i.e., lead to a model with two bands with opposite Chern numbers. Experimentally, the $\mathcal{C}_2$ breaking is provided through the alignment of one of the graphene layers with its substrate of hexagonal boron nitride, which, at leading order, creates a staggered mass term Δ_{AB}.

The band structure of twisted bilayer graphene aligned with hexagonal boron nitride thus involves two almost flat bands, separated by a small gap of order Δ_{AB}, which have Chern numbers $C = \pm 1$. These bands have a fourfold degeneracy, due to the spin and valley degrees of freedom. Chern numbers are equal in opposite spin copies, but opposite in opposite valleys, since the two valleys are connected by time-reversal conjugation. Combining the topology with the flatness of the bands leads to the valley and spin polarization of the system at integer fillings of either band through quantum Hall ferromagnetism, as explained above. Experimentally, one observes a quantized Hall conductance, even at zero magnetic field [30]. In twisted bilayer MoTe2, there are no Dirac cones to start with, so the origin of topology is different, and rather comes from the non-trivial coupling between the two layers, which introduces a winding of the Bloch states [33]. Likewise, there is a spontaneous spin-valley polarization due to quantum Hall ferromagnetism, thanks to the flatness of the band if the twist angle is tuned properly [31].

References

[1] K. v. Klitzing, G. Dorda, and M. Pepper, Phys. Rev. Lett. **45**, 494 (1980)

[2] K.S. Novoselov, Z. Jiang, Y. Zhang, S.V. Morozov, H.L. Stormer, U. Zeitler, J.C. Maan, G.S. Boebinger, P. Kim, and A.K. Geim, Science **315**, 1379 (2007)

[3] C.L. Kane and E.J. Mele, Phys. Rev. Lett. **95**, 146802 (2005)

[4] A. Altland and M.R. Zirnbauer, Phys. Rev. B **55**, 1142 (1997)

[5] M.J. Moessner R.: *Topological Phases of Matter* (Cambridge University Press, 2021)

[6] T.H.B.A. Bernevig: *Topological Insulators and Topological Superconductors* (Princeton University Press, 2013)

[7] C. Nayak, S.H. Simon, A. Stern, M. Freedman, and S. Das Sarma, Rev. Mod. Phys. **80**, 1083 (2008)

[8] M.V. Berry, Proc. Roy. Soc. A **392**, 45 (1984)

[9] R. Bianco and R. Resta, Phys. Rev. B **84**, 241106(R) (2011)

[10] Q. Niu, D.J. Thouless, and Y.-S. Wu, Phys. Rev. B **31**, 3372 (1985)

[11] M.B. Hastings and S. Michalakis, Commun. Math. Phys. **334**, 433 (2014)

[12] T. Fukui, Y. Hatsugai, and H. Suzuki, J. Phys. Soc. Jpn. **74**, 1674 (2005)

[13] D.J. Thouless, M. Kohmoto, M.P. Nightingale, and M. den Nijs, Phys. Rev. Lett. **49**, 405 (1982)

[14] R.B. Laughlin, Phys. Rev. B **23**, 5632(R) (1981)

[15] B.I. Halperin, Phys. Rev. B **25**, 2185 (1982)

[16] J. Dalibard, Collège de France Lecture Series (2017–2018)

[17] P.G. Harper, Proc. Phys. Soc. A **68**, 874 (1955)

[18] D.R. Hofstadter, Phys. Rev. B **14**, 2239 (1976)

[19] C.R. Dean, L. Wang, P. Maher, C. Forsythe, F. Ghahari, Y. Gao, J. Katoch, M. Ishigami, P. Moon, M. Koshino, T. Taniguchi, K. Watanabe, K.L. Shepard, J. Hone, and P. Kim, Nature **497**, 598 (2013)

[20] D. Jaksch and P. Zoller, New J. Phys. **5**, 56 (2003)

[21] M. Aidelsburger, M. Atala, M. Lohse, J.T. Barreiro, B. Paredes, and I. Bloch, Phys. Rev. Lett. **111**, 185301 (2013)

[22] H. Miyake, G.A. Siviloglou, C.J. Kennedy, W.C. Burton, and W. Ketterle, Phys. Rev. Lett. **111**, 185302 (2013)

[23] F.D.M. Haldane, Phys. Rev. Lett. **61**, 2015 (1988)

[24] M. König, S. Wiedmann, C. Bruüne, A. Roth, H. Buhmann, L.W. Molenkamp, X.-L. Qi, and S.-C. Zhang, Science **318**, 766 (2007)

[25] C.-Z. Chang, J. Zhang, X. Feng, J. Shen, Z. Zhang, M. Guo, K. Li, Y. Ou, P. Wei, L.-L. Wang, Z.-Q. Ji, Y. Feng, S. Ji, X. Chen, J. Jia, X. Dai, Z. Fang, S.-C. Zhang, K. He, Y. Wang, L. Lu, X.-C. Ma, and Q.-K. Xue, Science **340**, 167 (2013)

[26] J.G. Checkelsky, R. Yoshimi, A. Tsukazaki, K.S. Takahashi, Y. Kozuka, J. Falson, M. Kawasaki, and Y. Tokura, Nat. Phys. **10**, 731 (2014)

[27] X. Kou, S.-T. Guo, Y. Fan, L. Pan, M. Lang, Y. Jiang, Q. Shao, T. Nie, K. Murata, J. Tang, Y. Wang, L. He, T.-K. Lee, W.-L. Lee, and K.L. Wang, Phys. Rev. Lett. **113**, 137201 (2014)

[28] R. Yu, W. Zhang, H.-J. Zhang, S.-C. Zhang, X. Dai, and Z. Fang, Science **329**, 61 (2010)

[29] G. Jotzu, M. Messer, R. Desbuquois, M. Lebrat, T. Uehlinger, D. Greif, and T. Esslinger, Nature **515**, 237 (2014)

[30] M. Serlin, C.L. Tschirhart, H. Polshyn, Y. Zhang, J. Zhu, K. Watanabe, T. Taniguchi, L. Balents, and A.F. Young, Science **367**, 900 (2020)

[31] F. Xu, Z. Sun, T. Jia, C. Liu, C. Xu, C. Li, Y. Gu, K. Watanabe, T. Taniguchi, B. Tong, J. Jia, Z. Shi, S. Jiang, Y. Zhang, X. Liu, and T. Li, Phys. Rev. X **13** (2023)

[32] N. Bultinck, S. Chatterjee, and M.P. Zaletel, Phys. Rev. Lett. **124** (2020)

[33] F. Wu, T. Lovorn, E. Tutuc, I. Martin, and A.H. MacDonald, Phys. Rev. Lett. **122**, 086402 (2019)